

SIMULATIONS OF MAGNETOHYDRODYNAMICS INSTABILITIES IN INTRACLUSTER MEDIUM INCLUDING ANISOTROPIC THERMAL CONDUCTION

TAMARA BOGDANOVIĆ^{1,4}, CHRISTOPHER S. REYNOLDS¹, STEVEN A. BALBUS², AND IAN J. PARRISH^{3,5}

¹ Department of Astronomy, University of Maryland, College Park, MD 20742-2421, USA; tamarab@astro.umd.edu, chris@astro.umd.edu

² École Normale Supérieure, Laboratoire de Radioastronomie, 24 rue Lhomond, 75231 Paris CEDEX 05, France; steven.balbus@lra.ens.fr

³ Astronomy Department and Theoretical Astrophysics Center, 601 Campbell Hall, University of California, Berkeley, CA 94720, USA; iparrish@astro.berkeley.edu

Received 2009 May 29; accepted 2009 August 24; published 2009 September 21

ABSTRACT

We perform a suite of simulations of cooling cores in clusters of galaxies in order to investigate the effect of the recently discovered heat flux buoyancy instability (HBI) on the evolution of cores. Our models follow the three-dimensional magnetohydrodynamics of cooling cluster cores and capture the effects of anisotropic heat conduction along the lines of magnetic field, but do not account for the cosmological setting of clusters or the presence of active galactic nuclei (AGNs). Our model clusters can be divided into three groups according to their final thermodynamical state: catastrophically collapsing cores, isothermal cores, and an intermediate group whose final state is determined by the initial configuration of magnetic field. Modeled cores that are reminiscent of real cluster cores show evolution toward thermal collapse on a timescale which is prolonged by a factor of ~ 2 – 10 compared with the zero-conduction cases. The principal effect of the HBI is to re-orient field lines to be perpendicular to the temperature gradient. Once the field has been wrapped up onto spherical surfaces surrounding the core, the core is insulated from further conductive heating (with the effective thermal conduction suppressed to less than 10^{-2} of the Spitzer value) and proceeds to collapse. We speculate that, in real clusters, the central AGN and possibly mergers play the role of “stirrers,” periodically disrupting the azimuthal field structure and allowing thermal conduction to sporadically heat the core.

Key words: conduction – convection – galaxies: clusters: general – instabilities – MHD – plasmas

Online-only material: color figures

1. INTRODUCTION

The temperature structure of the intracluster medium (ICM) in central regions of galaxy clusters is bimodal. The non-cooling core clusters have isothermal ICM cores with low densities and hence long radiative cooling times. On the other hand, the central regions of the ICM in cooling core clusters have radiative cooling times that can be as short as 10^8 yr. Within the cooling radius (the location where the radiative cooling time is comparable to the Hubble time and hence the age of the cluster), the temperature decreases with decreasing radius (Peterson & Fabian 2006). Given the short cooling time, it is profoundly puzzling that the cores of these clusters have not undergone a cooling catastrophe. The current paradigm is that the central active galactic nucleus (AGN) heats the ICM; this remains one of the most direct arguments for “AGN feedback.” However, early work (Binney & Cowie 1981) highlighted the possible role that thermal conduction may play in these clusters.

Our understanding of the action of thermal conduction in atmospheres such as the ICM is undergoing a revolution. Because the ICM plasma is very dilute, thermal conduction will act in a very anisotropic manner, occurring essentially unchecked along magnetic field lines but being very strongly suppressed perpendicular to field lines. This elementary fact has profound implications for the dynamics and structure of the ICM (or, indeed, any dilute plasma atmosphere). As shown by Balbus (2000), the anisotropy of conduction fundamentally alters the Schwarzschild criterion for convection—rather than requiring an inverted *entropy* gradient, convection

in such an magnetohydrodynamic (MHD) atmosphere will occur whenever the *temperature* gradient is inverted, due to the *magneto-thermal instability* (MTI; see Parrish & Stone 2005, 2007, for the first numerical studies of this instability). Parrish et al. (2008) studied the effect of the MTI in the outer regions of clusters, where temperature decreases with radius, and found that the temperature profile of the ICM can be substantially modified on timescales of several billion years. The instability drives field lines to become preferentially radial leading to conduction at a high fraction of the Spitzer conductivity.

The ICM cores of cooling core galaxy clusters will be stable to the MTI (since the temperature in such cores is increasing with radius). However, Quataert (2008) has discovered a related instability (the *heat flux buoyancy instability*; HBI) which acts when the temperature is increasing with radius. Based on local simulations of the HBI in three-dimensional stratified atmosphere, Parrish & Quataert (2008) found the HBI induces MHD turbulence and can somewhat amplify the magnetic field in the plasma. They also discovered that, in the plane-parallel geometry that characterizes all local simulations, the instability saturates when the lines of magnetic field are re-oriented in such a way as to suppress the heat transport across the temperature gradient.

Guided by the results from the local simulations, Balbus & Reynolds (2008) suggested that MHD turbulence driven by the HBI may be important in regulating the conduction of heat into ICM cores and could mediate the stabilization of the cooling cores. They hypothesized that the presence of radiative cooling and the spherical (as opposed to planar) geometry would prevent field-line re-orientation from completely insulating the core from the conductive heat flux. They also highlighted the fact that HBI-driven turbulence would create a convective heat flux

⁴ Einstein Fellow.

⁵ Chandra Fellow.

that *removes* heat from the cool core (i.e., it acts as a cooling term in the energy equation).

In this paper, we present global models of cooling core clusters in which we explore the role of heat conduction and the HBI on the evolution of these cores. The results of our simulations suggest that the HBI alone cannot regulate and stabilize a cooling core. We have followed the nonlinear evolution of the HBI in the inner $\sim \text{few} \times 100$ kpc in clusters, and found that it is ubiquitous and rearranges the lines of the magnetic field in such a way that they are wrapped around the core. This results in dramatic suppression of the heat conduction below the Spitzer value. Consequently, within context of these simple models (which do not include AGNs or realistic cluster/dark matter dynamics), heat conduction can significantly delay but cannot prevent the catastrophic core collapse in real clusters. In Section 2, we briefly review the equations and timescales governing the problem of heat conduction in cluster cores as well as the numerical setup used in simulations. In Section 3, we present results from a parameter space study of cooling core clusters and then focus on a specific model of a core resembling that in the Perseus cluster. We discuss our results, approximations, and observational consequences in Section 4, and present our conclusions in Section 5.

2. SIMULATIONS

Using the three-dimensional MHD code *Athena* (Stone et al. 2008), we have carried out simulations of thermally conducting ICM cores which incorporate the effects of anisotropic thermal conduction. We run two classes of simulations. Firstly, we conduct a suite of simulations aimed at mapping out the behavior of clusters as a function of position in the two-dimensional parameter space $(t_{\text{cool}}/t_{\text{dyn}}, t_{\text{cond}}/t_{\text{dyn}})$, where the cooling timescale t_{cool} , conduction timescale t_{cond} , and dynamical timescale t_{dyn} are defined in Section 2.3. These simulations describe “theorist clusters” in the sense that no particular physical parameters (e.g., density, temperature and timescales) are implied, with only dimensionless ratios being relevant. We shall refer to these as our “parameter space survey simulations.” Second, we shall conduct simulations that are specifically tailored to describe physically realistic clusters. We shall refer to these as our “physical clusters/simulations.”

We must note one peculiarity of these (or indeed any) simulations of “idealized” galaxy clusters. In removing our model clusters from their cosmological setting, the computational complexity of the problem is reduced enormously. Indeed, it is currently infeasible to perform a cosmological simulation which resolves the small-scale physics relevant to our study. However, it is important to realize that galaxy clusters are dynamically young objects and, through the accretion of subclusters and groups, are still in the process of forming. Any ab initio model for the thermodynamic state of the ICM *must* acknowledge the cosmological setting. Neglecting the cosmological setting has two consequences for our work. First, real systems will possess dynamics related to merging substructures that is not captured in our treatment. The effects of neglecting this phenomenon will be discussed in Section 4. Second, there is no well-defined choice of “physical initial conditions” for our model clusters. We must be content with forming well-defined initial conditions that describe gross aspects of the systems under consideration. We describe our choice of initial conditions below. The fact that our results agree well with those of Parrish et al. (2009), who employ a rather different choice of initial condition, suggests a robustness to these choices.

2.1. Equations

The fundamental equations of the analysis are

$$\frac{\partial \rho}{\partial t} + \nabla \cdot (\rho \mathbf{v}) = 0 \quad (1)$$

$$\rho \frac{\partial \mathbf{v}}{\partial t} + \rho (\mathbf{v} \cdot \nabla) \mathbf{v} = \frac{(\nabla \times \mathbf{B}) \times \mathbf{B}}{4\pi} - \nabla p + \rho \mathbf{g}, \quad (2)$$

$$\frac{\partial \mathbf{B}}{\partial t} = \nabla \times (\mathbf{v} \times \mathbf{B}), \quad (3)$$

$$\frac{\partial e}{\partial t} + \nabla \cdot (e \mathbf{v}) = -p \nabla \cdot \mathbf{v} - \nabla \cdot \mathbf{Q} - n_e^2 \Lambda(T), \quad (4)$$

where ρ is the mass density, \mathbf{v} is the fluid velocity, \mathbf{B} is the magnetic field vector, \mathbf{g} is the gravitational acceleration, p is the gas pressure, e is internal energy density, \mathbf{Q} is the heat flux, and $\Lambda(T)$ is a cooling function, n_e is the electron number density, and T is the temperature. We adopt an equation of state $p = (\gamma - 1)e = \rho T / \mu m_p$, with $\gamma = 5/3$, adequate for monoatomic gas. We have ignored viscous terms in the equation of motion in this work; these will be considered in a future study.

In the absence of magnetic fields, we take the electron thermal conductivity to be given by its Spitzer value (Spitzer 1962):

$$\chi = \chi_s \approx \frac{1.84 \times 10^{-5} T^{5/2}}{\ln \lambda} \text{erg s}^{-1} \text{cm}^{-1} \text{K}^{-1}, \quad (5)$$

where the Coulomb logarithm $\ln \lambda$ is ~ 30 – 40 for conditions in a cluster cooling flow. The local conductive heat flux will then be given by $\mathbf{Q} = -\chi \nabla T$. If such efficient conduction operated unimpeded, radiative losses within massive ICM cores would be more than balanced by the conduction of heat from the outer portions of the ICM in all but the lowest mass clusters. This would eliminate the possibility of a cooling flow or, indeed, any significant departure from isothermality (Binney & Cowie 1981; Fabian et al. 2002; Voigt et al. 2002). However, magnetic fields of any plausible astrophysical strength will strongly suppress transport of electrons across their line of force. Thermal conduction is expected to be efficient along field lines, and suppressed perpendicular to the field lines. The form of the heat flux under these conditions is

$$\mathbf{Q} = -\chi \hat{\mathbf{b}} (\hat{\mathbf{b}} \cdot \nabla T), \quad (6)$$

where $\hat{\mathbf{b}}$ is a unit vector in the direction of the magnetic field. Assuming a spherical temperature gradient, the radial heat flux can be expressed as $\mathbf{Q} \cdot \hat{\mathbf{r}} = -\chi (\hat{\mathbf{b}} \cdot \hat{\mathbf{r}})^2 \partial T / \partial r$. For convenience, we will define a thermal diffusivity, $\kappa = \chi T / p = \kappa_{\text{aniso}} (n_0/n) (T/T_0)^{5/2}$, where κ_{aniso} has dimensions of a diffusion coefficient ($\text{cm}^2 \text{s}^{-1}$), and n_0 and T_0 are fiducial values for the electron number density and temperature, respectively.

Anisotropic thermal conduction is implemented in the *Athena* code via a split operator approach with subcycling (Parrish & Stone 2005). Subcycling ensures stability of the integration and is used whenever the Courant time step for conduction falls below that used for hydrodynamic equations. The thermal conduction time step is evaluated as $\delta t_{\text{cond}} = 0.5 (\delta x)^2 / \kappa_{\text{max}}$, where $\kappa_{\text{max}} = \kappa_{\text{aniso}}$ for $T_0 = 1$, and δx is the size of a resolution element. The thermal conduction term is implemented using the method of monotonized central difference limiters (Sharma & Hammett 2007) which prevents unphysical heat flow from

colder to hotter regions that may arise as a numerical artifact in a variety of algorithms.

In this work, we adopt two forms for the optically thin radiative cooling function; both are introduced into the *Athena* code using operator splitting as explicit source terms. The majority of our parameter space survey simulations employ a very simple “bremsstrahlung” form for the cooling function, $n_e^2 \Lambda = \alpha n^2 T^{0.5}$. We control the strength of radiative cooling and hence the cooling timescale via the parameter α . On the other hand, our physical cluster simulations use the Tozzi & Norman (2001) approximation for the cooling function that incorporates the effects of free–free and line cooling:

$$n_e^2 \Lambda = (C_1 (k_B T)^{-1.7} + C_2 (k_B T)^{0.5} + C_3) n_i n_e, \quad (7)$$

where $(k_B T)$ is in units of keV, and n_i is the ion number density. For mean metallicity of $Z = 0.3 Z_\odot$, $C_1 = 8.6 \times 10^{-3}$, $C_2 = 5.8 \times 10^{-2}$, and $C_3 = 6.4 \times 10^{-2}$, and the units of Λ are 10^{-22} erg cm³ s⁻¹. Mean molecular weight corresponding to this metallicity in case of a near complete ionization is $\mu = 0.59$.

2.2. Numerical Setup and Initial Conditions

The simulations were performed in a Cartesian coordinate system (x, y, z) with a cubic spatial domain defined by $x = \pm L/2$, $y = \pm L/2$, $z = \pm L/2$, where $L = 1$. Unless otherwise stated the nominal numerical resolution used is 100^3 .

All of our simulations have an initial density distribution that is described by a β -model, $\rho(r) = \rho_0 (1 + (r/r_0)^2)^{-0.75}$, where $r^2 = x^2 + y^2 + z^2$. The temperature distribution is initially isothermal with temperature T_0 . We choose to work in units where $\rho_0 = 1$, $r_0 = 0.1$, and $T_0 = 1$. The underlying gravitational potential is assumed to be dominated by the dark matter, and is static throughout the simulations with the form

$$\Phi = -\frac{3c_s^2}{4\gamma} \ln \left[1 + \left(\frac{r}{r_0} \right)^2 \right], \quad (8)$$

where c_s is the speed of sound corresponding to temperature T_0 . This form corresponds to hydrostatic equilibrium in the initial isothermal ICM density distribution.

The simplicity of an isothermal hydrostatic atmosphere makes it a compelling choice of initial condition. However, the astrophysical systems of interest have ICM cores that display a positive temperature gradient. Furthermore, the interesting dynamics is driven by temperature gradients. Thus, we employ a pre-cursor simulation where, starting from the isothermal state, we create a cool core in the atmosphere by allowing radiative cooling in the absence of conduction. This continues until the core reaches a temperature of $T_c \approx 0.3\text{--}0.4T_0$, similar to the range observed in cores. The density and magnetic field are allowed to evolve self-consistently during this initial cooling phase. We then use this cool-core state as the starting point for the full simulations (i.e., those including the anisotropic conduction and associated dynamics).

Note that cluster cores initialized in this way are not in thermodynamic equilibrium and that anisotropic conduction is not matched to exactly balance radiative cooling at the start of the full simulation (for alternative approach starting from thermodynamic equilibrium see Parrish et al. 2009). While realistic cluster cores are most likely not in thermodynamic equilibrium either, they experience more gradual thermal histories compared to that created in our simulations. We will discuss the effect of this feature later, along with the description of results.

The initial magnetic field strength is typically chosen so that the average value of the plasma parameter (i.e., the ratio of thermal pressure to magnetic pressure) is $\beta = 8\pi p/B^2 \sim 10^2\text{--}10^3$. We explore several different scenarios for the initial structure of magnetic fields. First, we define field-line geometry given by the form

$$B_x = \frac{B_0}{\sqrt{3}} \cos(\pi y) \cos(\pi z), \quad (9)$$

$$B_y = \frac{B_0}{\sqrt{3}} \cos(\pi x) \cos(\pi z), \quad (10)$$

$$B_z = \frac{B_0}{\sqrt{3}} \cos(\pi x) \cos(\pi y). \quad (11)$$

This initial geometry is self-consistently evolved within an isothermal core until field lines assume loosely tangled geometry while retaining the large-scale character given by the initial form. This field configuration is then used as a part of the initial conditions. These models are representative of an idealized scenario in which anisotropic conduction initially operates efficiently by transporting heat from the outer, hotter regions of a cluster to the cooler core center. Hereafter, we denote this class of models by “T.” In this model, the constant B_0 is the initial amplitude of the magnetic field. Second, we examine models with tangled purely azimuthal field lines, i.e., a field structure that is initially wrapped onto surfaces of constant r . In this scenario, we investigate the evolution of cool cores when the initial field geometry is set up to inhibit heat conduction toward the core. We use these models to test the hypothesis that spherical collapse and MHD turbulence driven by the heat flux instability can regulate field-line insulation and drive a reverse convective thermal flux (Balbus & Reynolds 2008). Defining a spherical polar coordinate system (r, θ, ϕ) , where $\theta = 0$ is aligned along the z -axis, we employ an azimuthal field structure defined by

$$B_\theta = 2B_0(1 + \sin(2\pi r/r_1)) \sin \theta \cos(2\phi), \quad (12)$$

$$B_\phi = 2B_0(1 + \sin(2\pi r/r_2)) \sin(3\theta) - B_0(1 + \sin(2\pi r/r_1)) \sin(2\phi) \sin(2\theta), \quad (13)$$

$$B_r = 0. \quad (14)$$

We refer to these as “A” models. Here, $B_0^2 = 8\pi p/\beta$, $r_1 = 0.1$, and $r_2 = 0.087$ are coherence lengths defining characteristic scales on which the magnetic field vector changes the direction. Finally, we examine a modification of the tangled azimuthal field model in which we include a radial component in the form of a split monopole

$$B_r = \text{sign} \frac{B_{r0}}{r^2 + \epsilon}, \quad \text{sign} = \begin{cases} 1 & \text{if } z > 0 \\ -1 & \text{otherwise.} \end{cases} \quad (15)$$

We shall refer to these as our “AR” models. The constant $\epsilon \ll r_0$ is a small number chosen to avoid a singularity at the origin. We use this simple setup to study cases in which the magnetic field at the very center of a cool core may be tangled and enhanced in the process of spherical collapse. We test to which extent such fields provide a local magnetic support as well as channel the heat within a small volume of the core. All initial magnetic field geometries are self-consistently evolved during the initial

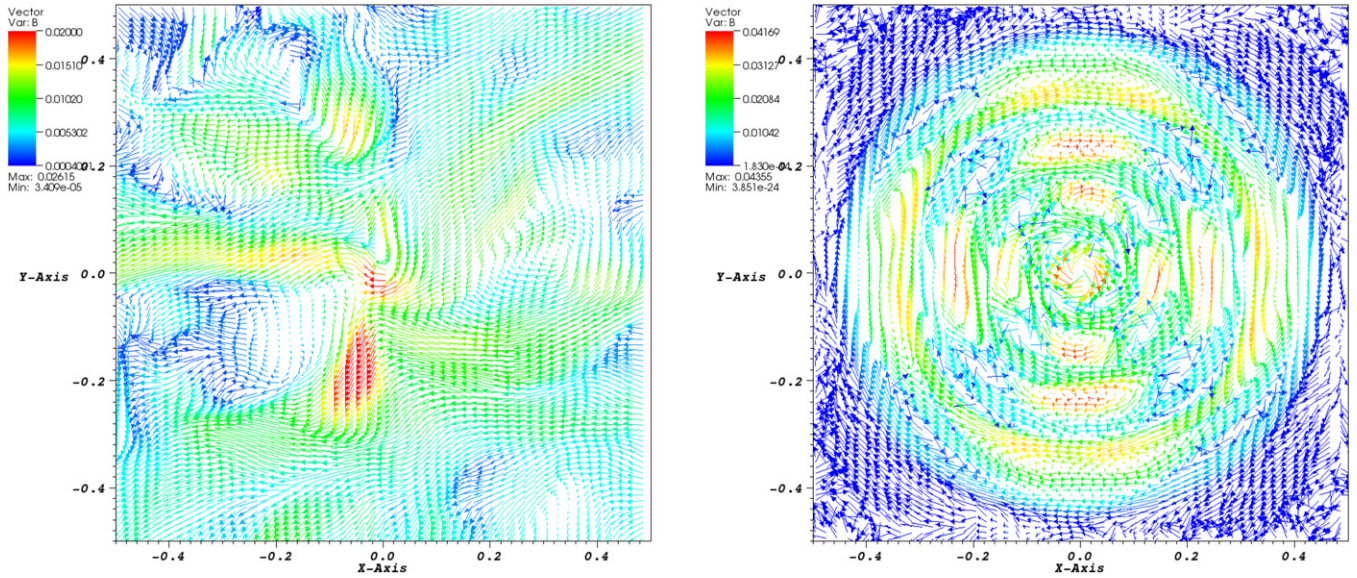


Figure 1. Examples of the geometry of magnetic field lines immediately after the initial radiative relaxation phase in which the cool core is imprinted into the initial conditions. Left: large-scale, loosely tangled magnetic field lines used as a part of initial conditions in T-models. Right: tangled azimuthal field lines with spatially variable ϕ and θ components used in A-models. Fields lines in AR-models appear very similar except for the addition of the split monopole term at the center. Both panels show the slice through the x - y -plane of a cluster center. Arrows mark the direction of magnetic field vectors, and colors indicate field strength. The orientation of vectors in the corners of figure representing A-model is the visualization artifact that arises for very weak fields.

(A color version of this figure is available in the online journal.)

precursor simulation in which the cool core is imprinted into the initial condition. For illustration, slices through the “T” and “A” field geometries (at a time just after the initial radiative relaxation of the model cluster) are shown in Figure 1.

We complete the specification of our simulations by describing the boundary conditions. The velocity boundary conditions at the interface of the active and ghost zones are zero-gradient outflow, and the pressure and density of the gas are extrapolated from the active zone into the ghost zone so as to maintain hydrostatic equilibrium in the ghost zones. This choice of boundary conditions ensures stability and prevents spurious sound waves from developing at the boundaries. The temperature is fixed to the virial temperature T_0 on a spherical shell at a radius $r = L/2$. Thus, while the dynamics are followed in the full cubical domain, only the interior of the $r = L/2$ sphere is physically interesting. Early experimentation with applying temperature boundary conditions at the edge of the cubic domain revealed behavior that appeared to depend upon the overall orientation of our Cartesian domain. Thus, we chose to impose thermal boundary conditions on a spherical surface in order to emulate hot intercluster plasma surrounding the cool core.

2.3. Characteristic Timescales

For our parameter space survey, we catalog our simulated clusters according to their characteristic dynamical, conduction, and cooling timescales. These are defined (in code units) by

$$t_{\text{dyn}} = \frac{R}{c_s} \approx \frac{0.39}{\sqrt{\mu}}, \quad (16)$$

$$t_{\text{cond}} = \frac{R^2 T_0}{\kappa \Delta T} \approx \frac{0.036}{\kappa_{\text{aniso}} \mu}, \quad (17)$$

$$t_{\text{cool}} = \frac{e}{n_e^2 \Lambda} \approx 0.27 \frac{\mu}{\alpha}, \quad (18)$$

where t_{dyn} is calculated for the cooling core radius $R = L/2 = 0.5$ and the average speed of sound in the region with virial temperature $T_0 = 1$, $\gamma = 5/3$, and $\mu = 1$ or 0.59 , as specified for a given run. When calculating t_{cool} , we evaluated the shortest timescale corresponding to the core center where typically $T_c \approx 0.3$ and $\rho_c \approx 3$ at the beginning of a simulation. In Equation (17), κ was evaluated for an average density in the core region $\langle \rho \rangle = 0.1$ and virial temperature.⁶ According to the theory of linear growth applied to the weak magnetic field regime, the plasma is unstable to HBI on the local dynamical time whenever the vector of the magnetic field is aligned with the temperature gradient and unbridled conduction is allowed in the direction of gravity. In the limit when lines of the magnetic field are preferentially oriented across the temperature gradient, this condition is modified by a factor $(\hat{\mathbf{b}} \cdot \hat{\mathbf{r}})$ in such way that

$$t_{\text{HBI}} = \left(\frac{d \ln T}{dr} \frac{d \Phi}{dr} \right)^{-1/2} \left| \hat{\mathbf{b}} \cdot \hat{\mathbf{r}} \right|^{-1}, \quad (19)$$

(Quataert 2008). For the values of the initial magnetic field used in simulations the Alfvén timescale is typically much longer with respect to the above timescales and thus, Alfvén waves are not expected to play a significant role during the phase characterized by the HBI instability and radiative cooling.

3. RESULTS

We have performed an extensive suite of simulations. Our primary set of 36 simulations (our parameter space survey simulations) represents a systematic exploration of the dependence of the cluster core evolution on ratios of the characteristic timescales (i.e., $t_{\text{cool}}/t_{\text{dyn}}$ and $t_{\text{cond}}/t_{\text{dyn}}$), and the magnetic field geometry. The cooling and conduction timescales are controlled via the parameters α and κ_{aniso} . Table 1 defines this set of models.

⁶ Note that the expression commonly used in literature to estimate t_{cond} omits factor $T_0/\Delta T$ and thus, refers to the shortest timescale for heat conduction.

Table 1
Value of κ_{aniso} in Models

Model	B-Field Structure	B1 ^a ($\alpha = 0$)	B2 ($\alpha = 0.01$)	TN ^b ($\alpha \approx 0.1$)	B3 ($\alpha = 0.3$)	B4 ($\alpha = 1$)
1	T				0.1	
2	T	0.025	0.025		1	1
3	T	0.05	0.05		10	10
4	A	0.01				
5	A	0.025	0.025	0.0	0.1	
6	A	0.1	0.05	0.1	1	1
7	A	1		1	10	10
8	AR	0.01	0.01	0.01		
9	AR	0.025	0.025	0.025	0.1	
10	AR			0.1	1	1
11	AR			1	10	10

Notes.

^a B1–4: models with the bremsstrahlung cooling function, $n_e^2 \Lambda = \alpha n^2 T^{0.5}$, and $\mu = 1$.

^b TN: models with the Tozzi–Norman cooling function for metallicity $Z = 0.3 Z_\odot$ and $\mu = 0.59$.

We explore three field geometries (the T, A, and AR geometries of Section 2.2) and five cooling laws (B1–4+TN; this includes the zero-cooling case $\alpha = 0$). For each choice of field geometry and cooling law, two to four simulations are performed with different degrees of thermal conduction. Thus, we can map out the behavior of clusters as a function of their position on the two-dimensional parameter space ($t_{\text{cool}}/t_{\text{dyn}}$, $t_{\text{cond}}/t_{\text{dyn}}$) and, furthermore, assess whether the initial field geometry can influence/change the eventual state of the cluster for a given position on the ($t_{\text{cool}}/t_{\text{dyn}}$, $t_{\text{cond}}/t_{\text{dyn}}$)-plane. We refer to individual models from Table 1 according to their alphanumeric tag consisting of the letter abbreviation corresponding to the magnetic field structure (T, A, or AR), a model number (1–11), and the descriptor of the cooling function (B1–B4 or TN). According to this convention, a model with a purely azimuthal initial magnetic field geometry, $\kappa_{\text{aniso}} = 0.025$, and no radiative cooling is marked as A5B1. *Note that this study includes but it is not limited to the part of the parameter space occupied by realistic clusters.*

We expect the HBI to be active; hence, one could readily envisage a scenario in which field-line re-orientation (by the HBI) completely insulates the central region from the conductive heat flux, which would prevent complete equilibration of core. However, as we shall see, while field-line re-orientation does occur, it never completely insulates the core. Figure 2 shows the models on the two-dimensional parameter space ($t_{\text{cool}}/t_{\text{dyn}}$, $t_{\text{cond}}/t_{\text{dyn}}$). The results of our simulations clearly divide this parameter space into three regions depending upon the ratio $t_{\text{cool}}/t_{\text{cond}}$. If $t_{\text{cool}}/t_{\text{cond}} \gtrsim 10^2$, cooling appears to be too weak to sustain any significant temperature gradient against the action of conduction, and all simulated cluster cores become approximately isothermal. On the other hand, if $t_{\text{cool}}/t_{\text{cond}} \lesssim 25$, our simulated clusters always undergo a cooling catastrophe, although it can be appreciably delayed by the action of HBI-regulated conduction. In the intermediate regime ($25 \lesssim t_{\text{cool}}/t_{\text{cond}} \lesssim 10^2$), clusters can evolve to either an isothermal state or undergo a cooling catastrophe depending upon the initial magnetic field configuration. These are the only outcomes; none of our simulated clusters achieved a non-isothermal quasi-steady state.

In the rest of this section, we shall describe these results in detail and, in particular, examine the role of the HBI in influencing the thermal evolution of the cluster core.

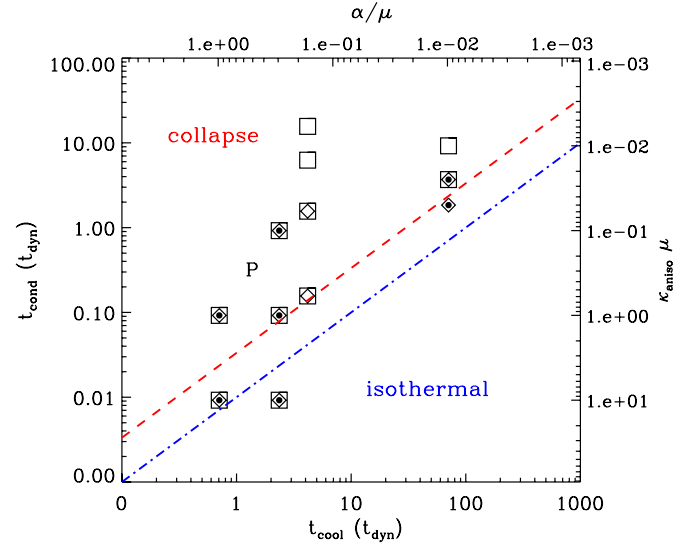


Figure 2. Illustration of the parameter space of clusters explored in this study shown in terms of cooling and heat conduction time, normalized to the dynamical time. Also marked are corresponding values of κ_{aniso} and α (for a list of values used in simulations see Table 1). Filled circles, diamonds, and squares represent T, A, and AR-models, respectively. A combination of symbols signifies that different magnetic field configurations were simulated at the same value of α and κ_{aniso} . Letter “P” marks the location of the Perseus-like model. The investigated parameter space includes but it is not limited to that of realistic clusters which occupy the range $1 \lesssim t_{\text{cool}}/t_{\text{dyn}} \lesssim 10$ and $\text{few} \times 0.1 \lesssim t_{\text{cond}}/t_{\text{dyn}} \lesssim 10$.

(A color version of this figure is available in the online journal.)

3.1. Clusters with an Isothermal Final State

As an extreme case, we first describe the evolution of cool cores in models without radiative cooling, $\alpha = 0$ (also referred to as “B1” models). The fact that these clusters evolve to an isothermal state is not as trivial as it first appears. Recall that our full-up simulations start with a cool core (and hence a positive temperature gradient) already imprinted on the ICM atmosphere. We expect the HBI to be active and, hence, one could readily envisage a situation in which field-line re-orientation by the HBI completely insulates the core from the conductive heat flux and hence prevents complete equilibration of the core. As we will see, field-line re-orientation does indeed occur but never completely insulates the core.

Table 2 (B1 column) shows the time taken for each of the non-cooling models to achieve an approximately isothermal state. Cores with loosely tangled field lines, captured in T-models, evolve to isothermal state on significantly shorter timescales with respect to the cores in models A and AR, where the field-line geometry is preferentially azimuthal. Figure 3 shows the evolution of the core temperature and mean angle between magnetic field lines and the radius unit vector, \hat{r} , in three models representing different magnetic field geometries, T2B1, A5B1, and AR9B1, all at the same value of $\kappa_{\text{aniso}} = 0.025$. The core temperature was measured at the center of the core, whereas the angle $\langle \theta_B \rangle$ is calculated as a volume average of $\cos^{-1}(\hat{b} \cdot \hat{r})$, and it indicates the alignment of the field lines with the global temperature gradient.⁷ As expected, the action of the HBI is most apparent in the tangled field model (T2B1) where we see a rapid re-orientation of the field lines from $\langle \theta_B \rangle \approx 57^\circ$ to $\langle \theta_B \rangle \approx 71^\circ$. The corresponding effective thermal conductivity

⁷ The region of the cluster core outside of $0.3 L$ is not taken into account in the calculation of $\langle \theta_B \rangle$, in order to focus on the field structure closer to the core center and avoid effects of the boundaries.

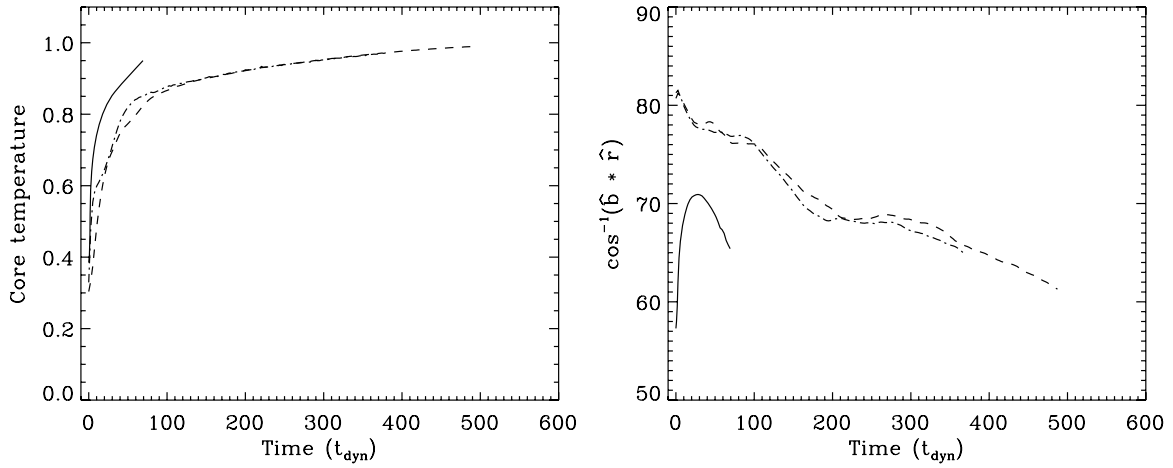


Figure 3. Left: evolution of the core temperature in T2B1 (solid), A5B1 (dashed), and AR9B1 (dash-dot) models, respectively. Right: evolution of the mean angle, $\langle \theta_B \rangle$, between the lines of the magnetic field and the radius unit vector (same models), indicating the alignment of the field lines with the global temperature gradient.

Table 2

Time Scale (in t_{dyn}) for Core Evolution Towards Collapse (C) or Isothermal State (I)

Model	B-Field Structure	B1 ($\alpha = 0$)	B2 ($\alpha = 0.01$)	TN ($\alpha \approx 0.1$)	B3 ($\alpha = 0.3$)	B4 ($\alpha = 1$)
1	T				12 (C)	
2	T	70 (I)	> 1000 (C)		80 (C)	10 (C)
3	T	60 (I)	80 (I)		< 3 (I)	< 3 (I)
4	A	> 500 (I)				
5	A	500 (I)	380 (C)	30 (C)	8 (C)	
6	A	240 (I)	510 (C)	160 (C)	18 (C)	5 (C)
7	A	50 (I)		> 700 (I) ^a	20 (I)	13 (C)
8	AR	> 500 (I)	420 (C)	90 (C)		
9	AR	500 (I)	560 (C)	110 (C)	8 (C)	
10	AR			230 (C)	20 (C)	5 (C)
11	AR			> 700 (U) ^b	20 (I)	25 (C)

Notes.

^a A7TN: evolution of the core that initially headed toward collapse was reversed to evolution toward the isothermal state.

^b AR11TN: the final state for this model appears undetermined (U) at the end of the simulation.

is $(\hat{\mathbf{b}} \cdot \hat{\mathbf{r}})^2 \approx 0.25$ of the Spitzer value but decreases as the field lines are re-oriented. Once the core has equilibrated, the HBI is no longer driven and the field lines become more disoriented again leading to a final value between $\langle \theta_B \rangle \approx 60^\circ - 70^\circ$. A similar final field orientation results in the A- and AR-models (i.e., the azimuthal initial field configurations). In these cases, the core takes substantially longer to equilibrate, however, with the initial heat flux corresponding to only ~ 0.02 of the Spitzer value. In comparison, the timescale for unbridled conduction in this set of models is $t_{\text{cond}} \approx 3.7 t_{\text{dyn}}$.

Given the same initial geometry of magnetic field lines, the cores with higher values of κ_{aniso} evolve toward isothermality on shorter timescales. The behavior of models shown in Figures 4 and 5 confirms this general expectation, summarized in Equation (17). Figure 4 shows the evolution of the core temperature and orientation of the magnetic field lines in T-models, T2B1, and T3B1. Similarly, Figure 5 shows the evolution for four A-models, A4B1, A5B1, A6B1, and A7B1.

Interestingly, these non-cooling cores remain rather kinematically quiescent throughout the entire evolution, and the magnetic field does not play a significant role in subsequent dynamical evolution of the core. Figure 6 shows that the early evolution of

the magnetic and kinetic energy density exhibit different behaviors in T- and A-models. In the T-models, the volume-averaged magnetic and kinetic energy increase over time due to the action of the HBI; it appears that a weak and short-lived dynamo may be established. The A- and AR-models, on the other hand, show a monotonic decrease in the kinetic and magnetic energy densities as the non-equilibrium azimuthal magnetic fields relax and numerically reconnect. In both panels the components of energy density are normalized to the internal energy density of the gas and, hence, the kinetic and magnetic energy represent a small fraction ($\sim 10^{-4}$) of the internal energy. This implies that cores are kinematically quiescent and that even after it has been enhanced (T-models), the magnetic field is not sufficiently strong to be dynamically important.

In fact, these qualitative results are borne out even when there is cooling present provided it is weak and much slower than the heat conduction in the sense that $t_{\text{cool}}/t_{\text{dyn}} > 10^2$. Examples of such behavior are models T3B3, A7B3, and AR11B3, all of which evolve toward isothermal final state.

3.2. Clusters Which Undergo Catastrophic Collapse

Real cooling core galaxy clusters do not have isothermal ICM atmospheres and hence, while this avoids the cooling catastrophe, it must not be considered a physical outcome. The more interesting case are those clusters in which cooling is too effective to allow an isothermal state to be achieved. As already mentioned, all of our model clusters with $t_{\text{cool}}/t_{\text{dyn}} < 25$ undergo an eventual cooling catastrophe; Table 2 lists the time taken for the model clusters to either undergo catastrophic collapse (C) or equilibrate to an isothermal state (I). We now discuss the collapsing clusters in more detail.

To illustrate many of the dynamical aspects of these collapsing clusters, we discuss run T2B2 in detail. Figure 7 (solid line) shows the evolution of the core temperature together with the average field-line orientation for run T2B2. At $t = 0$, the core is not in a state of thermal balance, with conductive heating overwhelming the radiative cooling. The core is rapidly heated from $T \approx 0.4T_0$ almost to a state of isothermality ($T \approx 0.85T_0$). The HBI is clearly playing a role during this early heating event, as revealed by the rapid re-orientation of the field geometry toward an azimuthal configuration (Figure 8). After this early heating event, an approximate balance between conductive heating and radiative cooling is maintained for a

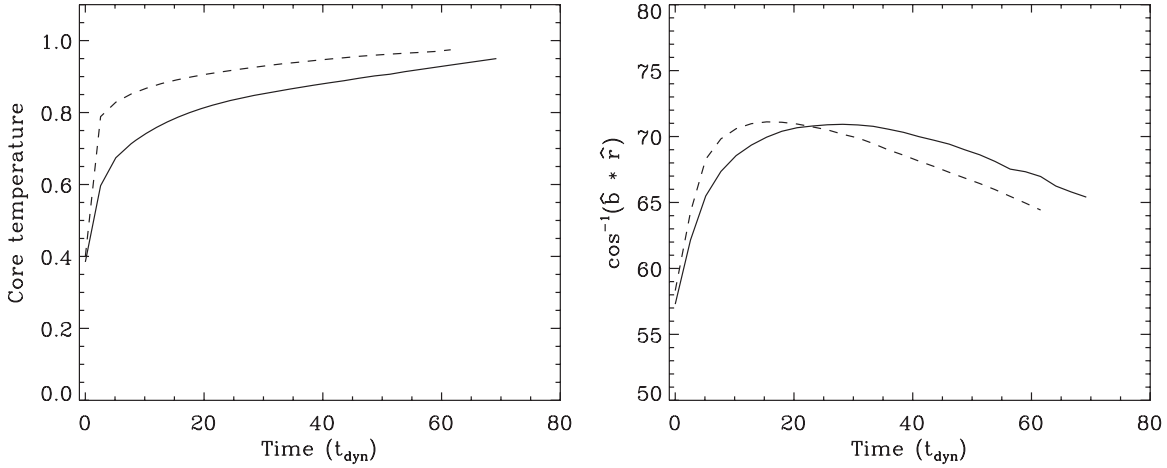


Figure 4. Left: evolution of the core temperature in T2B1 (solid) and T3B1 (dashed) models, respectively. Right: evolution of the $\langle \theta_B \rangle$ for the same two models.

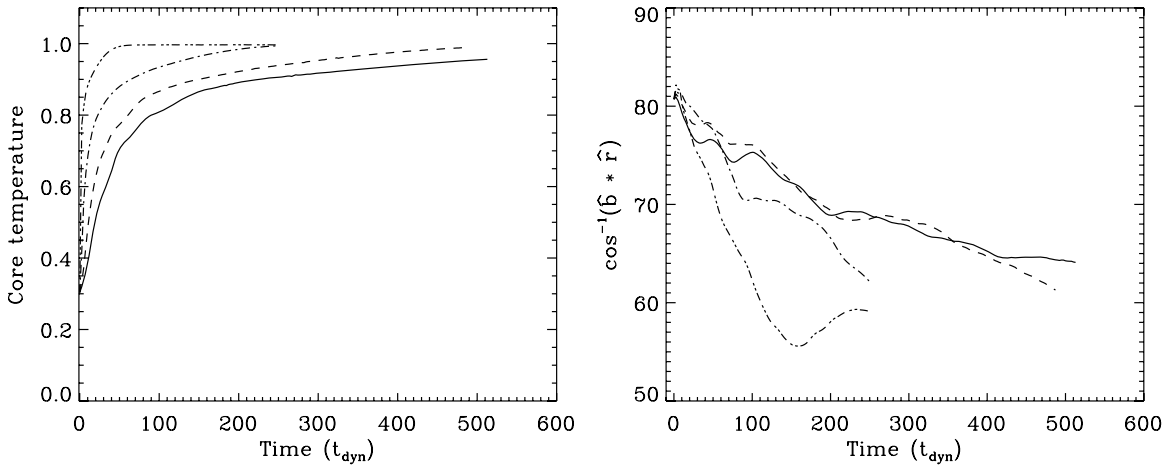


Figure 5. Left: evolution of the core temperature in four A-models: A4B1 (solid), A5B1 (dashed), A6B1(dash-dot), and A7B1 (dash-3-dot), respectively. Right: same four models, evolution of $\langle \theta_B \rangle$.

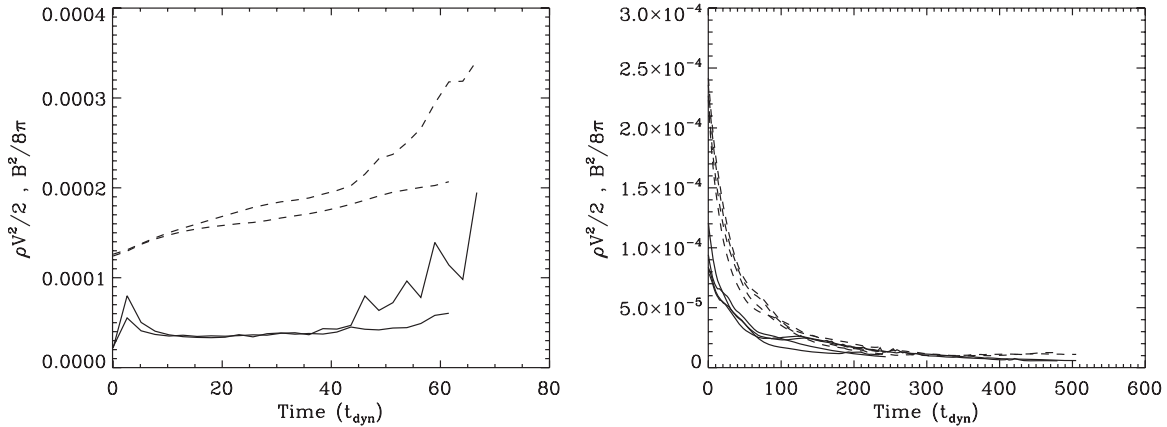


Figure 6. Evolution of the kinetic (solid) and magnetic (dashed) energy density in two T-models shown in Figure 4 (left) and four A-models from Figure 5 (right) without radiative cooling. Both components of energy density are normalized to the instantaneous internal energy density.

duration of $\sim 300t_{\text{dyn}}$. Eventually, azimuthal field-line wrapping reduces the conductive heat flux to the point where the core temperature starts to decrease. This slow collapse will end in a cooling catastrophe, in this case at some time $t > 1000t_{\text{dyn}}$. For comparison, the nominal cooling timescale for this group of models set by the value of α and calculated according to Equation (18) is $t_{\text{cool}} \approx 69t_{\text{dyn}}$. Thus, we see that thermal conduction can dramatically increase the time taken for the

cluster to undergo the cooling catastrophe even when the HBI is inducing azimuthal field-line wrapping within the cluster core.

As may be expected, cores with initially loosely tangled fields (T-models) evolve toward collapse on timescales longer than cores with initially azimuthal fields (A- and AR-models).⁸

⁸ Even in the A-model, the field configuration at the start of the full simulation is not perfectly azimuthal due to field distortions imprinted during the precursor simulation in which the cool core is formed.

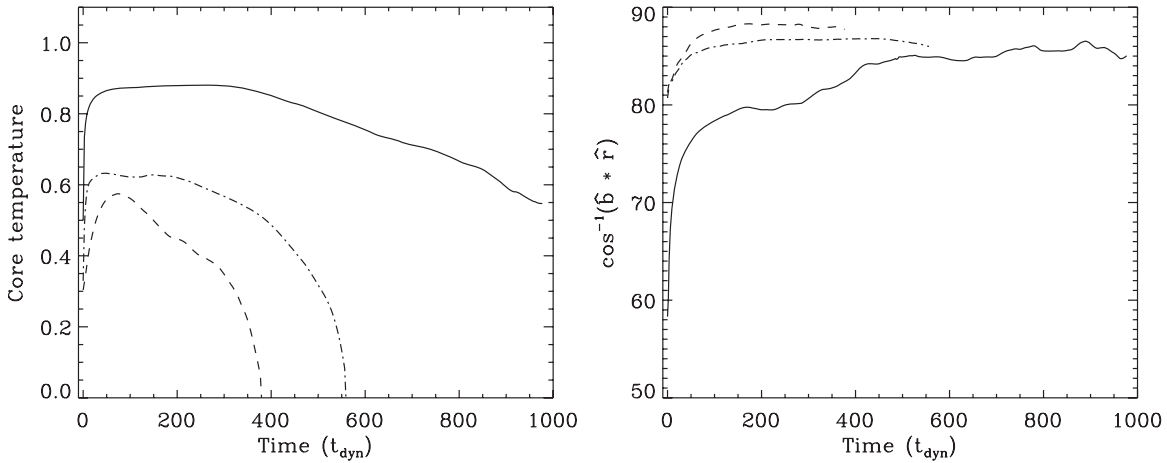


Figure 7. Left: evolution of core temperature in models with different magnetic field structure, all with $\kappa_{\text{aniso}} = 0.025$ and $\alpha = 0.01$: T2B2 (solid), A5B2 (dashed), and AR9B2 (dash-dot). The nominal cooling timescale for this group of models set by the value of α is $t_{\text{cool}} \approx 69 t_{\text{dyn}}$. Right: same models, evolution of magnetic field orientation.

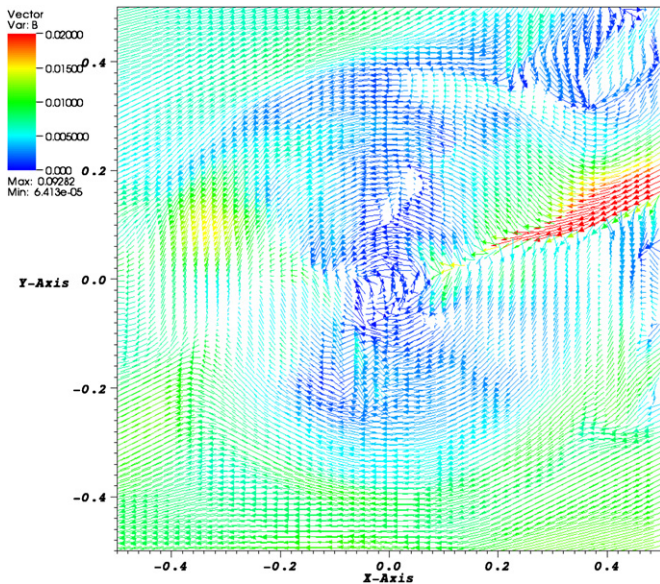


Figure 8. Final orientation of the magnetic field lines in model T2B2, 800 dynamical times after the beginning of the simulation. Large-scale, loosely tangled magnetic field lines with $\langle \theta_B \rangle = 58^\circ$ are used as a part of the initial conditions in this model, as illustrated in the left panel of Figure 1. Traces of the initial topology are still present at late times in the strongest component of the field; however, most of the lines are wrapped around the core as a consequence of HBI. The final value of $\langle \theta_B \rangle = 85^\circ$. Figure shows a slice through the x - y -plane of a cluster center.

(A color version of this figure is available in the online journal.)

Furthermore, the AR-model clusters (which include a split monopole term to the initial field configuration and hence possess a significant radial field in the core regions) have a collapse that is delayed with respect to A-models. Figure 7 compares the evolution of core temperature and $\langle \theta_B \rangle$ in models T2B2, A5B2, and AR9B2, characterized by different initial magnetic field structure and identical cooling and conduction ($\kappa_{\text{aniso}} = 0.025$ and $\alpha = 0.01$). In A and AR-models, the field orientation starts at $\langle \theta_B \rangle \approx 80^\circ$; this permits sufficient conductive heat flux to raise the core temperature to $T \approx 0.5\text{--}0.6T_0$. However, the action of the HBI further increases the field-line orientation to $\langle \theta_B \rangle > 85^\circ$ and insulates the core which proceeds to collapse. The cores in models A5B2 and AR9B2 collapse in 380 and 560 dynamical times after the beginning of

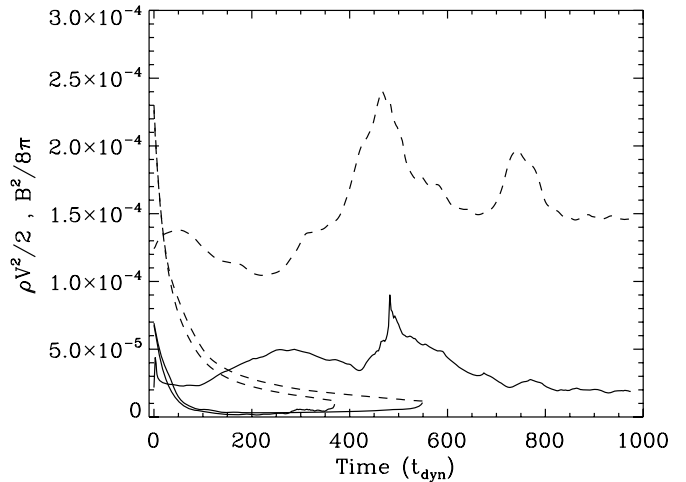


Figure 9. Evolution of the kinetic (solid) and magnetic (dashed) energy density for models T2B2 (ending at $1000 t_{\text{dyn}}$), A5B2 ($380 t_{\text{dyn}}$), and AR9B2 ($560 t_{\text{dyn}}$). Both components of energy density are normalized to instantaneous internal energy density and comprise a small fraction of it.

the simulation, respectively, compared with the collapse on a timescale of $> 1000 t_{\text{dyn}}$ for model T2B2.

As was the case for the non-cooling clusters, the modeled cooling cores remain kinematically quiescent, and the magnetic field never plays a direct dynamical role. The evolution of kinetic and magnetic energy density for models T2B2, A5B2, and AR9B2 is shown in Figure 9. The kinetic and magnetic energy are a small fraction of the internal energy of the gas and the core region. Velocities remain very subsonic, $v < 10^{-2} c_s$. Independent of the assumed initial geometry of the field lines, the HBI does not result in significant field amplification.

The fact that the cores remain (relatively) kinematically quiescent results in very little convective heat flux. To see this, Figure 10 shows the evolution of the radial convective, conductive, and advective heat flow for models T2B2 and A5B2 within a sphere of radius $r = 0.1$ along with the total radiative loses and the fiducial value of unbridled conductive heat luminosity at the Spitzer value, for comparison. To construct these quantities, we start with the radial components of the advective, convective, and conductive heat fluxes defined by

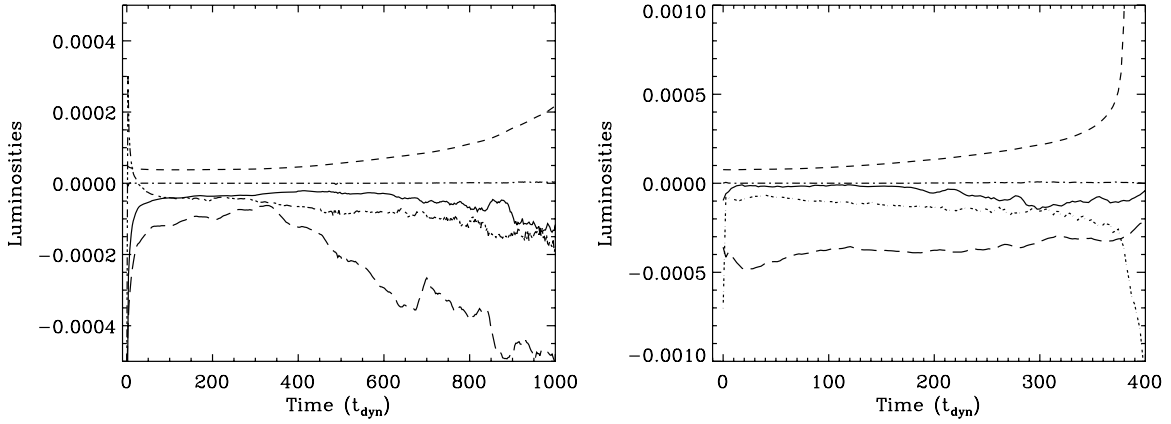


Figure 10. Evolution of luminosity components in models T2B2 (left panel) and A5B2 (right) measured within the sphere of radius of 0.1 from the center of the cluster. Each component is marked with a different line: anisotropic heat conduction (solid), radiative (dashed), convective (dash-dot), advective (dash-3dot), and fiducial value of unbridled heat conduction at the Spitzer value (thick, long-dashed), all in arbitrary units. The heat flux at the full Spitzer value was divided by the factors of 5 (left panel) and 10 (right) in order to show it alongside of other components. Negative fluxes are inflowing and vice versa.

$$Q_{adv} = \frac{\gamma}{\gamma - 1} k_B \langle \langle n \rangle \langle T \rangle \langle v_r \rangle + \langle T \rangle \langle \delta n \delta v_r \rangle \rangle, \quad (20)$$

$$Q_{conv} = \frac{\gamma}{\gamma - 1} k_B \langle \langle v_r \rangle \langle \delta n \delta T \rangle + \langle n \rangle \langle \delta n \delta T \rangle + \langle \delta n \delta T \delta v_r \rangle \rangle, \quad (21)$$

$$Q_{cond} = -\chi (\hat{\mathbf{b}} \cdot \hat{\mathbf{r}})^2 \partial T / \partial r. \quad (22)$$

Here, v_r is the radial component of the velocity field. The fluctuations (δv_r , δn , δT) were defined as relative to a mean calculated on the surface of the sphere. We then integrate these components across the surface of the spherical shell $r = 0.1$ to obtain relevant luminosities plotted in Figure 10. The convective heat flux acts as a cooling term for the core (Balbus & Reynolds 2008) but remains significantly smaller than the other heat fluxes. As expected, the conductive heat component initially decreases as the HBI wraps the lines of the magnetic field around the core. At later times ($t > 600 t_{\text{dyn}}$), it starts increasing again as a consequence of radial field-line stretching in the process of core collapse, which once again “unlocks” heat conduction along the temperature gradient. Note that trends in evolution of luminosity components in T- and A-models appear qualitatively similar; however, there is about an order of magnitude difference in the magnitude of conductive luminosity between the two. This is a consequence of an early, efficient suppression of anisotropic heat conduction by magnetic field lines in model A5B2 in comparison to T2B2. In both runs the field lines eventually saturate at an angle of $\langle \theta_B \rangle \approx 85^\circ - 88^\circ$, in such a way suppressing the conductive heat flux to a fraction of only $(\hat{\mathbf{b}} \cdot \hat{\mathbf{r}})^2 \approx 10^{-3}$ of the Spitzer value throughout the core volume. Apart from unbridled heat conduction, the largest of the remaining four components of luminosity in both models is the radiative cooling. In terms of luminosity magnitudes, radiative cooling is followed by advective luminosity which can be interpreted as heating of the core in the process of adiabatic compression, which is in turn followed by anisotropic conduction and convective luminosity.

As stated at the beginning of this section, the parameter space is occupied by three distinct groups of systems which end up in either catastrophic collapse ($t_{\text{cool}}/t_{\text{cond}} \lesssim 25$), isothermal state ($t_{\text{cool}}/t_{\text{cond}} \gtrsim 10^2$), or as border line cases. Border line cases

represent the transition population between the collapse and isothermal group of objects, and their final state is determined by the structure of the magnetic field. The behavior of borderline cases is illustrated by comparing models T3B2 and A6B2 (which differ only in their initial field structure), where the former evolves to the isothermal state in $80 t_{\text{dyn}}$ and the latter collapses after $510 t_{\text{dyn}}$. Another example is provided by models T3B4, A7B4, and AR11B4, of which only the core in the T-model evolves toward the isothermal state, while those in A- and AR-models collapse. Cores in models A7TN and AR11TN are also border line cases given that both evolve on very long timescales and that they seem to hang on a very edge between collapse and isothermality. Interestingly, the core in A7TN initially evolves toward collapse, but after $\sim 300 t_{\text{dyn}}$ the temperature curve reverses toward isothermal. The core temperature in AR11TN remains relatively flat until late time in the simulation and its final state undetermined. The cause of different outcomes in these two models is probably stochastic, driven by a slightly different evolution of the magnetic field, and it underlines the role of the field structure in these transition population of objects. The values of $t_{\text{cool}}/t_{\text{cond}}$ for TN, B2, and B4 border line cases are 26, 38, and 75, respectively. We also find that cores with $t_{\text{cool}}/t_{\text{cond}} < 25$ evolve toward collapse regardless of their initial field geometry (T2, A6, and AR10 in the case of both B3 and B4 runs but also T2B2 and A5B2), while those with $t_{\text{cool}}/t_{\text{cond}} \gtrsim 250$ all evolve toward the isothermal state (T3B3, A7B3, and AR11B3).

3.3. Models of Physical Clusters

In order to offer a more intuitive interpretation of the role of the HBI for a portion of the parameter space populated by real clusters, we present a second group of calculations where we scale simulation parameters specifically to match the cooling core of a rich galaxy cluster. We mark the position of these models with the letter “P” in $(t_{\text{cool}}, t_{\text{cond}})$ space in Figure 2. It is worth noting that characteristic timescales of real cooling core clusters occupy the range $1 \lesssim t_{\text{cool}}/t_{\text{dyn}} \lesssim 10$ and $\text{few} \times 0.1 \lesssim t_{\text{cond}}/t_{\text{dyn}} \lesssim 10$, which places them in the collapse region of Figure 2.

Specifically, we consider a cluster characterized by a virial temperature of $kT_0 = 7$ keV, initial core temperature of $kT_c \approx 3$ keV, and core radius of $R_0 = 100$ kpc; these properties are reminiscent of the Perseus cluster. The gas number density

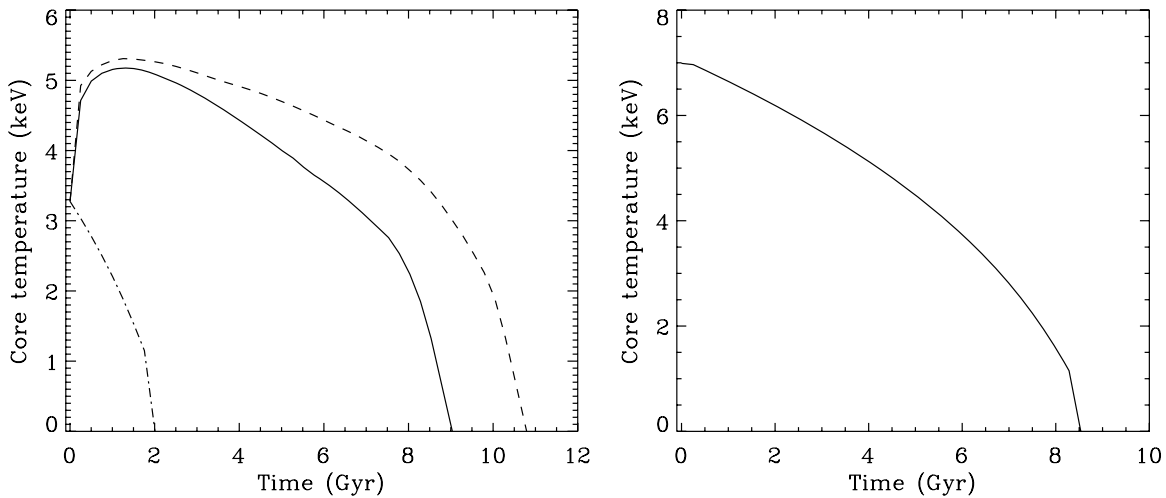


Figure 11. Left: evolution of temperature in the core of a cluster for models P1 (solid), P2 (dashed), and P5 (dash-dot) models. Right: same for P5 only, starting from an isothermal core at virial temperature of 7 keV.

Table 3
Models of Perseus-like Cluster

Model	B-Field Structure	Resolution (N^3)	κ_{aniso} (κ_{Spitz})	$\Delta t_{\text{collapse}}$ (Gyr)
P1	A	100	1	9
P2	AR	100	1	10.5
P3	A	200	1	8
P4	A	64	1	6
P5	A	100	0	2

in the modeled core is $n_0 = 0.03 \text{ cm}^{-3}$ (somewhat lower than in Perseus), and the speed of sound is $c_s \approx 900 \text{ km s}^{-1}$ in the core center. The core cools radiatively according to the Tozzi–Norman cooling function (Tozzi & Norman 2001). For this cluster, we ran a set of models spanning different magnetic field configurations and simulation resolutions, as detailed in Table 3. In this group of models, we test the evolution of the cores with predominantly azimuthal magnetic field geometry, a scenario that allows us to calculate a lower limit on the life time of conducting cores. With the exception of model-P5, the (anisotropic) heat conduction is set to the Spitzer value (Equation (5)) and mediated by the magnetic field in all models. Model-P5 is a pure radiative collapse model ($\kappa_{\text{aniso}} = 0$) given for comparison. The (initial) characteristic timescales for this system are $t_{\text{dyn}} \approx 1.3 \times 10^8 \text{ yr}$, $t_{\text{cond}} \approx 4.1 \times 10^7 \text{ yr}$, and $t_{\text{cool}} \approx 2 \text{ Gyr}$. We assume initial values of plasma parameter and the strength of the radial component of the magnetic field to be $\beta = 10^3$, $B_r = 0$ and $B_r = 3\mu G$, for A- and AR-models, respectively.

The collapse of conducting cores is postponed by a factor of ~ 2 – 10 with respect to the timescale for pure radiative collapse. The cores in models P1 and P2 evolve through an initial heating of the core during which time the HBI re-orientates the field lines in order to reduce the conductive heat flux. Figures 11 and 12 show the evolution of the core temperature and $\langle \theta_B \rangle$ in P1- and P2-models along with the pure radiative collapse case, for comparison. The core with the initial temperature of $\sim 3 \text{ keV}$, in the absence of heat conduction heads toward collapse in only $t_{\text{cool}} \approx 2 \text{ Gyr}$ (model P5). The cores in P1 and P2 models evolve through the initial rise in temperature, have a phase of uniform evolution approximately linear with time, and in the final 2 Gyr dominated by radiative cooling behave similarly to

the pure radiative collapse case. As remarked in the previous section, the initial rise in the core temperature in models with heat conduction is a consequence of non-equilibrium initial conditions. The intermediate phase of steady, quasi-linear decay of the core temperature is specific to conducting cores and is absent in the case of a pure collapse model. The presence of the HBI is indicated by the high value of $\langle \theta_B \rangle = 87^\circ$ shown in the left panel of Figure 12, in contrast to the pure radiative collapse scenario P5 (right panel) which does not maintain the azimuthal structure of the field. The field-line re-orientation appears to saturate at $\langle \theta_B \rangle \approx 87^\circ$ and, from then on, the core undergoes a gradual decline in core temperature until it reaches a temperature of $kT \sim 2$ – 3 keV . After that time, the core temperature decreases more rapidly due to the onset of line cooling within the TN-cooling function, and the cooling catastrophe is reached $\sim 2 \text{ Gyr}$ later. Indeed, this final stage in the conducting core models is very similar to the pure radiative collapse case, conduction having very little effect.

If real cluster cores are similar to the cores modeled here, they are likely to be observed precisely during the long gradual decline phase (although compared with model clusters during this phase, real clusters have a larger fractional temperature decrease as one heads into the core). In model-P1, this phase starts from 1 Gyr after the beginning of the simulation (at which time the core has a temperature of 5 keV) and the core collapses 8 Gyr later. In model P2, the life time of the core is extended due to the presence of a split monopole, with collapse occurring 9.5 Gyr after the start of this decline phase. A pure cooling simulation starting from a temperature of 5 keV undergoes the cooling catastrophe in approximately 4 Gyr. Thus, even starting off with rather azimuthal field geometries, thermal conduction delays the thermal collapse of the cluster core by at least a factor of 2.

It follows from the findings in the previous section that the longest lived cooling cores are those with large-scale magnetic fields (represented by T-models). In order to estimate the factor by which core collapse is postponed in these models, we consult our grid of models outlined in Tables 1 and 2. It is possible to infer that T-model cores collapse on timescales 2–5 times longer with respect to the cores with predominantly azimuthal fields (A-models), as illustrated in examples of model pairs: T2B2–A5B2, T2B3–A6B3, and T2B4–A6B4. Hence, if T-model cores evolve 2–5 times longer than A-model cores, and Perseus-like

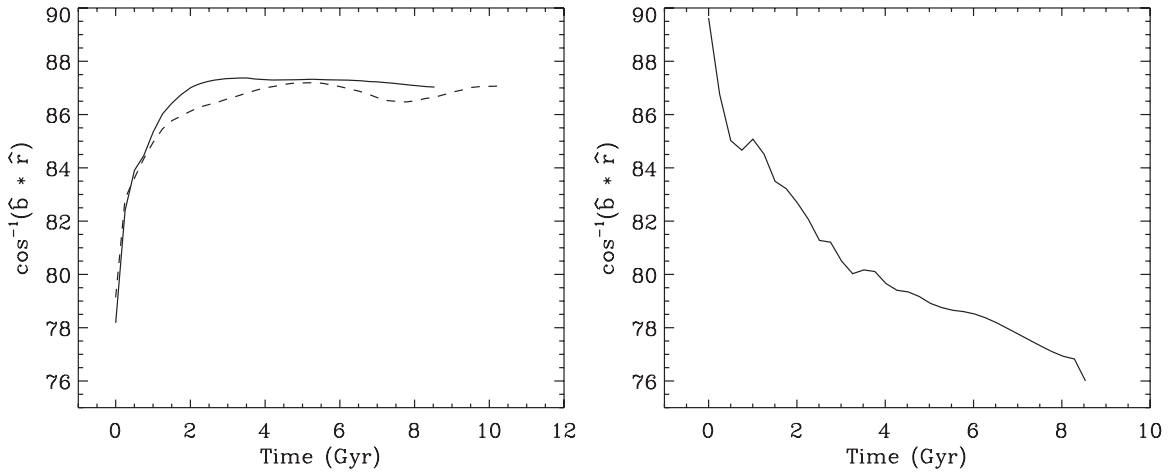


Figure 12. Left: evolution of $\langle\theta_B\rangle$ in P1 (solid) and P2 (dashed) models in the central 60 kpc region. Right: same, except for P4 model (pure radiative collapse). Spherical collapse in the absence of HBI leads to smaller $\langle\theta_B\rangle$ and does not maintain the azimuthal orientation of the magnetic field lines.

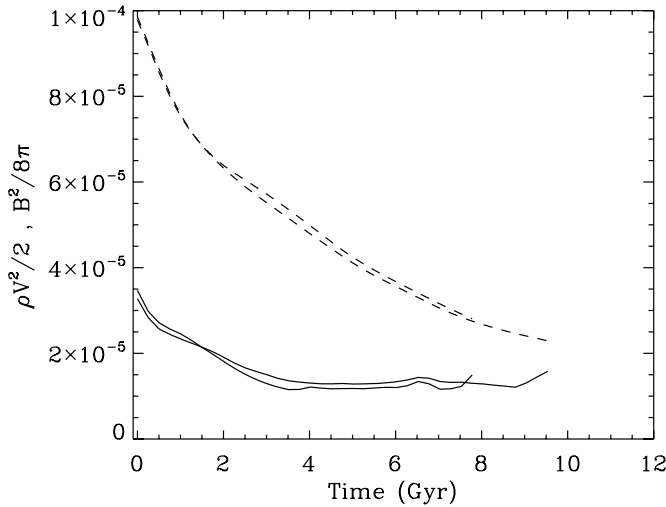


Figure 13. Evolution of mean kinetic (solid) and magnetic (dashed) energy density in P1 (shorter) and P2 (longer) normalized to mean instantaneous energy density.

A-model cores evolve on timescales $\sim 2 t_{\text{cool}}$, than the overall evolution of collapsing cores can be prolonged by a total factor of $\sim 2-10 t_{\text{cool}}$.

As found in Sections 3.1 and 3.2, these model clusters cores are characterized by an absence of strong turbulence or a magnetic dynamo effect. The magnetic and kinetic energies uniformly decrease in P1 and P2 models (Figure 13) and are only a small fraction of $\sim 10^{-5}-10^{-4}$ of the internal energy. Figure 14 shows the distribution of velocity magnitude in the x - y -plane containing the core center. The highest velocities in the core are of the order of 30 km s^{-1} and are visibly associated with the magnetic field structure. As the relative strength of the magnetic field decreases in the process of core collapse, the core center becomes kinematically more quiescent with respect to the initial velocity distribution.

Modeled Perseus-like cores exhibit the strongest heat conduction and heat flux buoyancy instability within the radius of $\sim 20 \text{ kpc}$ —a distance comparable to the half-depth radius of the core where the temperature gradient is steepest. Figure 15 shows the evolution of five luminosity components in units of erg s^{-1} calculated for a sphere of radius of 20 kpc in model

P1. Note that during the first $\sim 1 \text{ Gyr}$ of evolution, anisotropic heat conduction overcompensates for the radiative losses and that this phase is coincident with the initial rapid rise of the core temperature seen in Figure 11. Between 1 and 7.5 Gyr, radiative losses are comparable to but larger than the rate of heat conduction and in this period core temperature steadily declines. In the remaining period of evolution, the rate of radiative cooling becomes $\gtrsim 2$ times larger than the anisotropic heat conduction, and the core evolves toward collapse in the fashion similar to a pure radiative collapse scenario. The rate of energy transported by convection is consistently ~ 2 orders of magnitude lower than that of the anisotropic conduction, and it acts as a cooling term throughout the simulation. Also included in Figure 15 is the fiducial rate of unbridled heat conduction at the Spitzer value (thick, long dash line), plotted for comparison—because this component of luminosity is significantly larger than the others, we divided it by a factor of 10 in order to show it in the same plot.

Models P1, P3, and P4 constitute a crude numerical resolution study for these models. In order to characterize the effect of numerical resolution on our results, we choose the run P1 with the numerical resolution of 100^3 as a baseline model. With the tangled azimuthal field structure and characteristic coherence lengths of $r_1 = 0.1$ and $r_2 = 0.087$, this run is a good choice for resolution study, because the resolution effects are potentially more severe than in the runs with large scale, loosely tangled field. We carried out calculations equivalent to P1, at a higher resolution of 200^3 (run P3) and a lower resolution of 64^3 (run P4). Interestingly, we find that stepping up the numerical resolution leads to a non-monotonic evolution of the collapse timescale (Figure 16). This behavior can be explained by the effect of resolution on magnetic field orientation (right panel of Figure 16). Higher resolution captures the finer, radial structure of tangled field lines in addition to the dominant azimuthal component, resulting in the lower initial value of $\langle\theta_B\rangle$. This results in a highest rate of heat conduction in model P3 (0.04, 0.054, and 0.01 of the Spitzer value for P1, P3, and P4, respectively) and a more rapid re-orientation of the field lines due to HBI when compared to the moderate-resolution model P1. The consequence of rapid HBI evolution in the model core P3 is that it also collapses before the core in P1. On the other hand, heat conduction in model P4 is initially at such a low level that its evolution proceeds fairly similar to a pure

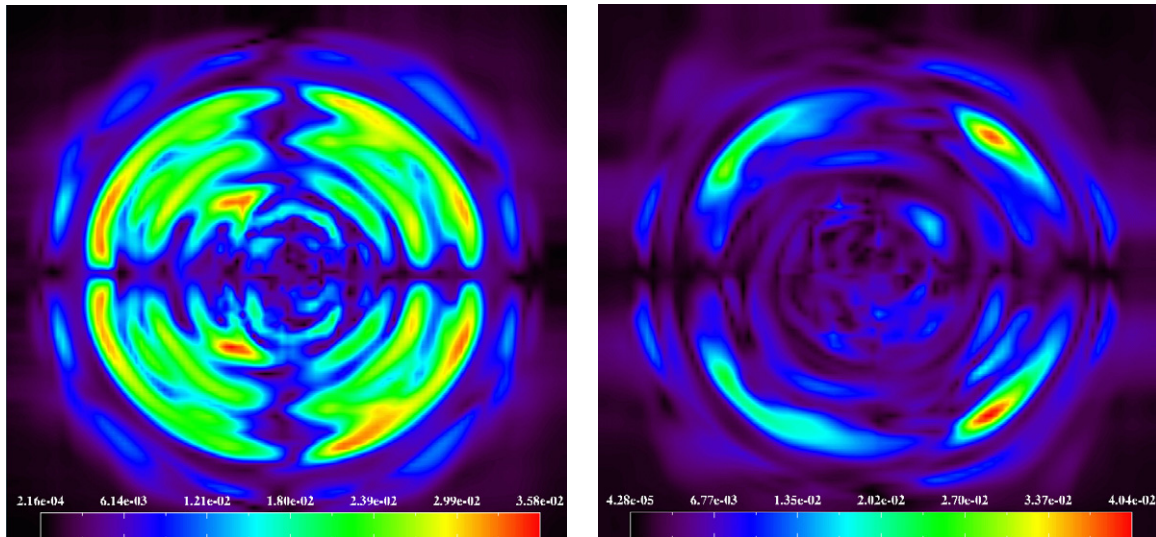


Figure 14. Snapshots from P1 model of the Perseus cluster showing the distribution of velocity magnitude at 500 Myr (left) and 3.5 Gyr (right) after the beginning of the simulation. Figures show the slice through the x - y -plane of a cluster center. A velocity unit corresponds to 820 km s^{-1} , implying that highest velocities are of the order of 30 km s^{-1} . The apparent symmetry in velocity distribution is a consequence of initial symmetry in magnetic field geometry.

(A color version of this figure is available in the online journal.)

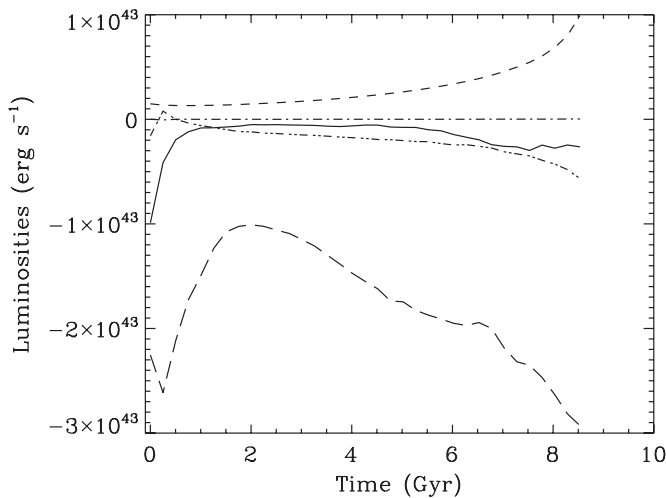


Figure 15. Evolution of luminosity components in model P1 measured within a sphere of radius of 20 kpc. Each component is marked with a different line: anisotropic heat conduction (solid), radiative (dashed), convective (dash-dot), advective (dash-3dot), and a fiducial value of unbridled heat luminosity at the Spitzer value (thick, long-dashed). The heat flux at the full Spitzer value was divided by a factor of 10 in order to show it alongside of other components. Negative fluxes are inflowing and vice versa.

radiative collapse and thus, occurs on a shorter timescale than in models P1 and P3. Progressing from the simulation with 64^3 resolution toward the higher end, the discrepancy in overall evolution time of the core decreases from ~ 2 Gyr to ~ 1 Gyr, indicating convergence. Based on this, we estimate that core evolution in most affected models in our calculations can be prolonged by ~ 1 Gyr.

4. DISCUSSION

Heat conduction is, in principle, capable of providing a large fraction of the energy necessary to prevent the core collapse in clusters of galaxies—indeed, the potential importance of conduction has been discussed ever since the realization that thermal collapse was a problem for ICM atmospheres (Binney &

Cowie 1981). However, attempts to solve the cooling flow problem with thermal conduction face several challenges. Because of a steep temperature dependence of Spitzer conductivity, heat conduction is expected to play a lesser role in low-mass clusters and groups of galaxies, where most of the gas is below 5 keV (Best et al. 2007; Zakamska & Narayan 2003). Even unbridled Spitzer thermal conduction cannot offset radiative losses in these low-mass systems. Hence, heat conduction cannot be a single solution to the cooling flow problem across the full range of masses, and additional sources of heat are needed to stabilize cooling flows in at least these lower mass systems. Even in hot systems where conduction is potent, previous studies have highlighted fine-tuning problems (Nulsen et al. 1982; Bregman & David 1988). Under the assumption that a tangled magnetic field essentially acts as a scalar suppression factor for isotropic conduction, and that the suppression factor f is a fixed parameter, Kim & Narayan (2003) show that f must be fine-tuned in order to obtain a thermal quasi-equilibrium resembling real cooling core clusters. Even then, this equilibrium is unstable with a growth time ~ 2 –5 Gyr.

Our results indicate that the presence of the HBI even further undermines the role of heat conduction because of its tendency to stifle conduction by rearranging the lines of the magnetic field to be orthogonal to the temperature gradient. We find that only systems with a large disparity in characteristic timescales, $t_{\text{cool}}/t_{\text{cond}} \gtrsim 10^2$, can avoid the cooling catastrophe by evolving to the isothermal state. Systems reminiscent of real clusters, with $t_{\text{cool}}/t_{\text{cond}} \lesssim 25$ evolve toward thermal collapse on timescales $\lesssim 10 t_{\text{cool}}$. For many cooling core clusters (such as Perseus), this is significantly shorter than a Hubble time, hence rendering heat conduction alone incapable of rescuing the core from collapse.

That said, we do find that conduction can significantly increase the time to thermal collapse, i.e., a significant energy is conducted into the core before the field-line re-orientation by the HBI seals it off and enables it to collapse. At this point, we must acknowledge the missing ingredients in our idealized cluster models. A quiescent cluster core can be significantly disturbed by cosmologically induced dynamics (e.g., subcluster mergers) and/or powerful outbursts from a central AGN. Either

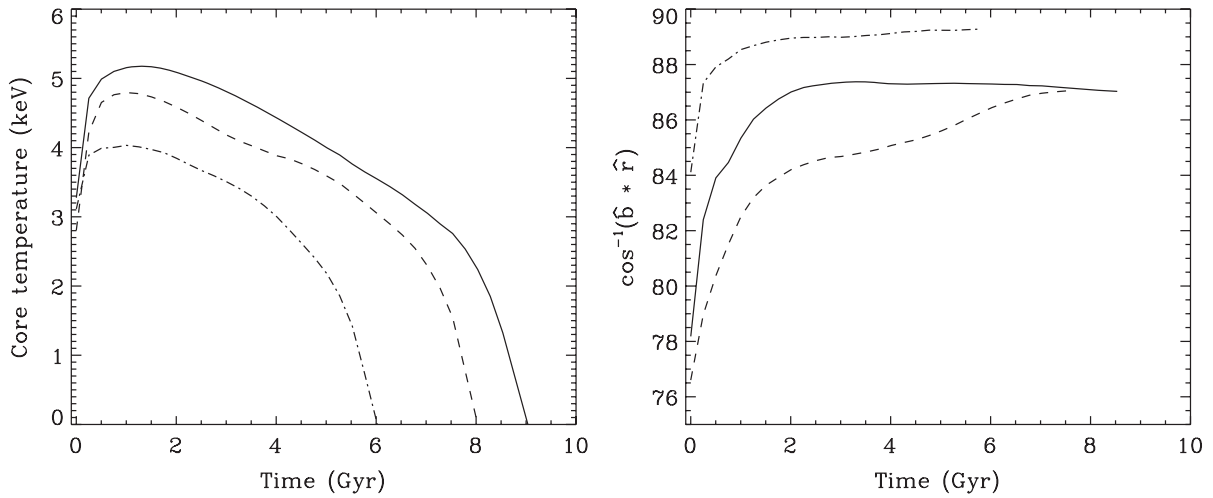


Figure 16. Effect of numerical resolution on evolution of the core temperature (left) and $\langle \theta_B \rangle$ (right) in P1 (solid), P3 (dashed), and P4 (dash-dot) runs carried out at resolution of 100^3 , 200^3 , and 64^3 , respectively.

of these events will disrupt the azimuthal nature of the field and may partially reset the evolution being described by our models. Thus, while thermal conduction seems unable to stabilize cooling cores alone, it may still be the primary agent heating cluster cores provided that it is *enabled* by subcluster mergers or AGNs. Note that this is a very different role than that normally envisaged for AGNs in cooling cluster clusters; if correct, *AGNs are stirrers and not heaters*.

An interesting property of our models is the absence of strong turbulent motions. With plasma motions at $\sim 10\text{--}30 \text{ km s}^{-1}$ modeled collapsing cores are kinematically quiescent in comparison with realistic cores, which exhibit turbulent velocities in the range $\sim 100\text{--}200 \text{ km s}^{-1}$ over comparable spatial scales (Conselice et al. 2001; Hatch et al. 2006). This highlights the necessary role of the central AGN and cluster mergers as stirrers of the intercluster plasma.

Both observational and theoretical studies of the cooling problem have established that the mechanism responsible for the stability of cooling cores has to be gentle, spatially distributed, and physically reminiscent of diffusion (Kim & Narayan 2003; Fabian et al. 2003). This is an intrinsic property of heat conduction but is more difficult to understand in pure AGN-heating scenarios. For example, simple shock heating by AGN jets fails to stabilize cooling flows in pure hydrodynamic simulations (Vernaleo & Reynolds 2006) unless a high degree of turbulent heat diffusion is postulated (Brüggen et al. 2009). In addition, Nagai et al. (2007) find that the entropy of the gas in cooling cores is surprisingly low—at 10s of keV cm^2 the gas is on a brink of catastrophic collapse and yet maintained in that state over a large fraction of the Hubble time. This presents a challenge for any mechanism which would heat the gas via strong turbulent motions or shocks, as it is expected to result in a much higher value of entropy than that observed. The implication of this discovery is that an unusually delicately balanced feedback mechanism operates in cooling cores and that heat conduction in combination with additional mechanisms may play an important role.

Another implication of the ubiquity of HBI is that clusters with cool cores may exhibit a characteristic magnetic field structure, where field lines are wrapped around the core and have a predominantly azimuthal structure. Although our model clusters

never completely forget about their initial magnetic field (i.e., T-models and A-models can be recognized even at late time), the wrapping of field lines into spherical shells is ubiquitous. The instability drives the field lines to almost orthogonal position with respect to the temperature gradient, $\langle \theta_B \rangle \approx 80^\circ\text{--}90^\circ$. This has several consequences. First, it creates exactly the kind of magnetic field geometry envisaged in models of AGN blown bubbles that invoke “magnetic draping” (Ruszkowski et al. 2007). In these models, a bubble of relativistic plasma which is buoyantly rising in the ICM atmosphere is stabilized to Rayleigh–Taylor and Kelvin–Helmholtz instabilities by a layer of strong magnetic field that has been swept up on its leading edge. It is suggested that this mechanism is responsible for the surprising stability of “ghost cavities” in the ICM of the Perseus cluster, and is an alternative to models that invoke plasma viscosity (Reynolds et al. 2005). Second, this characteristic field-line geometry leads to the most direct observable predictions/manifestations of the HBI in the ICM. Magnetic fields in the ambient ICM can be probed via the rotation measure (RM) of polarized radio sources in the background.

The RM is an integral measurement of the effect that magnetic fields impart on the orientation of the plane of an electromagnetic wave traveling through the plasma. Hence, an azimuthal field structure would produce a characteristic radial dependence in the observed RM: it would vanish at the projected cluster center, and peak at some projected radius within the cooling core. We calculate this effect for our Perseus-like models using the expression $\text{RM} = 812 \text{ rad m}^{-2} \int n_e \mathbf{B} \cdot d\mathbf{l}$, where n_e is the electron number density in units of cm^{-3} , \mathbf{B} is the vector of the magnetic field in units of μG , and \mathbf{l} is the depth of the magnetic screen in kiloparsecs. Figure 17 shows an illustrative calculation of the RM for model P2. We find that in Perseus-like models the magnetic field with mean strength of $\langle B \rangle \sim 0.1 \mu\text{G}$ produces RM of order $\sim 100 \text{ rad m}^{-2}$. The HBI-wrapped field also produces a characteristic spatial structure to the RM map. Future observatories with the radio instruments such as *Square Kilometer Array* should provide the sensitivity needed to identify and study background sources with sufficient areal density to map out these RM patterns. Note however that our calculation accounts for the RM arising from the core of a cluster but does not take into account the effect of magnetic

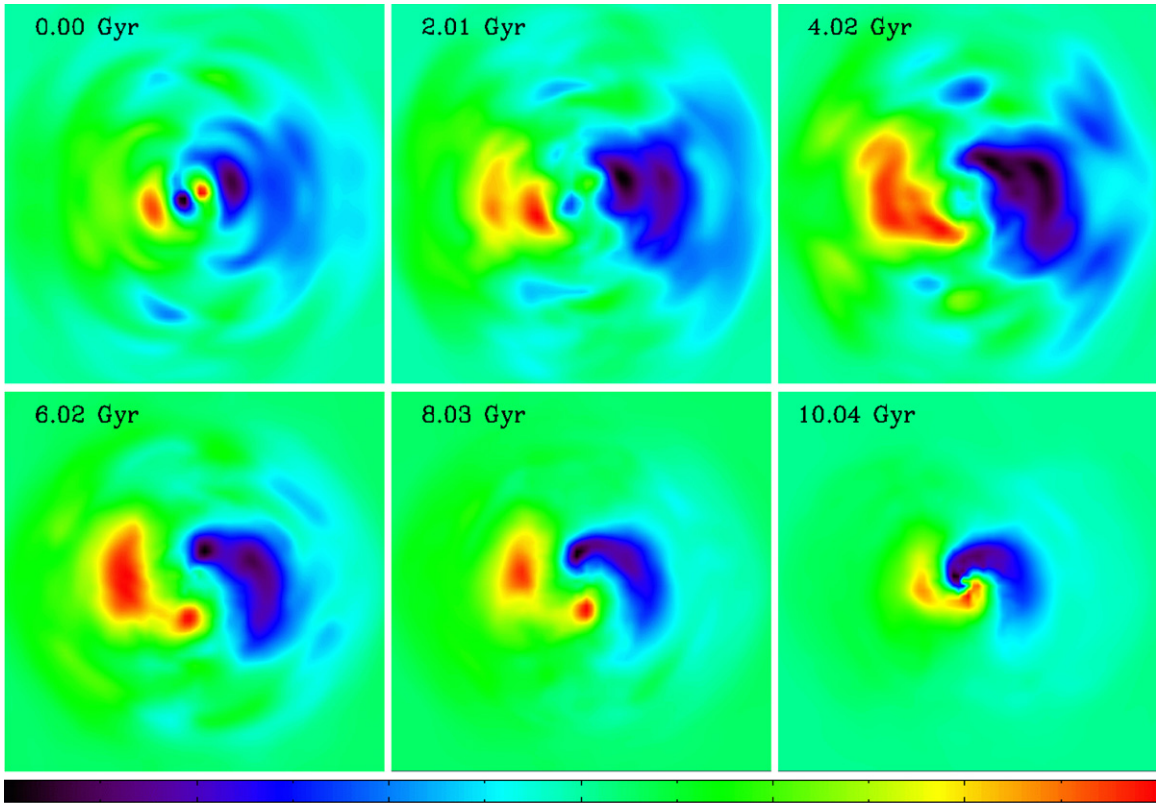


Figure 17. Rotation measure maps calculated for model P2 for a line of sight along x -axis. The color bar indicates the RM intensity which ranges from $(-\max, \max)$, where $\max = 150, 110, 95, 120, 170, 265 \text{ rad m}^{-2}$ for each panel in the time sequence, respectively.

(A color version of this figure is available in the online journal.)

structures and plasma in the outer parts of a cluster. Therefore, if the cluster field strength is dominated by the magnetic fields in the core, this effect may be measurable.

5. CONCLUSIONS

We have performed simulations of cooling cores in clusters of galaxies with the aim to study the role of anisotropic heat conduction and recently discovered HBI on the thermodynamic evolution of cores. Our models focus on the base state of cluster cores and do not take into account physics of the central AGNs or dark matter or ICM substructure resulting from hierarchical merging of subcluster units. We explore the parameter space of cooling and conduction timescales as well as different magnetic field configurations. We summarize our most important results as follows.

1. The parameter space of modeled systems can be divided into three distinct groups of models where collapsing cores occupy the parameter range $t_{\text{cool}}/t_{\text{cond}} \lesssim 25$ and isothermal cores exhibit $t_{\text{cool}}/t_{\text{cond}} \gtrsim 10^2$. The range between these two groups is occupied by a class of systems whose final state is determined by the configuration of magnetic field lines.
2. The efficiency of heat conduction along the lines of magnetic field ranges between $\sim 10^{-3}$ and 0.2 of the Spitzer value, depending on the initial structure of the magnetic field and evolutionary stage of the core.
3. Modeled conducting cores that correspond to real clusters, exhibit evolution toward core collapse slower by a factor of ~ 2 –10 with respect to the timescale for a pure radiative

collapse. For many cooling core clusters (such as Perseus), this is significantly shorter than a Hubble time, implying that heat conduction alone cannot rescue the core from collapse. The extent to which core collapse is postponed in our models is a function of the initial magnetic field topology, where systems with higher values of $t_{\text{cool}}/t_{\text{cond}}$ ratio and field configurations amenable to conduction result in longer collapse time scales.

4. Magnetic field lines in cores in which HBI is actively operating rearrange themselves in such way that the final value of $\langle \theta_B \rangle \approx 80^\circ$ – 90° . In contrast, cores that are not characterized by HBI have $\langle \theta_B \rangle \approx 60^\circ$ – 70° . If seen in observations, the alignment of field lines across the global temperature gradient would provide a strong evidence for the existence of MHD instabilities in clusters, which have so far only been considered theoretically.
5. Heat flux buoyancy instability operating in modeled cores is not characterized by a strong turbulence and results in kinematically quiescent cores. A related consequence of this property is that MHD turbulence driven by the heat flux instability does not drive a convective thermal flux sufficient to regulate the core collapse. This finding is interesting in light of observational and theoretical studies of the cooling problem which have established that the mechanism responsible for the stability of cooling cores has to be gentle and spatially distributed in order to agree with the low levels of entropy observed in some cooling cores and implies that heat conduction in combination with additional mechanisms may play an important role for the cooling problem.

The prospects for future work are numerous, and they stem from the need to design more realistic models of cooling cores and also to understand the interplay of MHD instabilities with other mechanisms operating in clusters. Future studies will be needed to address the evolution of cool core clusters within the cosmological framework and consider the effects of minor and major mergers on gas mixing, kinematically and MHD-driven turbulence, field-line tangling, AGN fueling, and the overall thermodynamic state of a cluster. On the other hand, they will also need to disentangle the effects of plasma transport processes and magnetic fields via simulations that incorporate full MHD as well as viscosity, thermal conduction, and cosmic ray diffusion.

Note that in parallel to this work, Parrish et al. (2009) carried out an independent study of cool cluster cores with HBI. Parrish et al. (2009) focus on a portion of the parameter space occupied by real clusters and consider the role of central entropy and AGN heating for the final thermodynamical state of a cluster core. Given different approaches, the two studies complement each other and in the areas of overlap arrive to similar conclusions.

We thank Sean O'Neill and Eve Ostriker for useful and insightful discussions. T.B. thanks the UMCP-Astronomy Center for Theory and Computation Prize Fellowship program for support. Support for T.B. was in part provided by NASA through the Einstein Fellowship Program, grant PF9-00061, awarded by the Chandra X-Ray Center, which is operated by the Smithsonian Astrophysical Observatory for NASA under contract NAS8-03060. T.B. and C.S.R. wish to acknowledge support from the NSF under grant AST-0908212. C.S.R. acknowledges support from the Chandra Theory and Modeling Program under grant TM7-8009X. S.A.B. has been supported by a grant from the Conseil Régional de l'Île de France. Support for I.J.P. was provided by NASA through Chandra Postdoctoral Fellowship Grant PF7-80049, awarded by the Chandra X-Ray Center, which is operated by the Smithsonian Astrophysical Observatory for NASA under contract NAS8-03060. Numerical simulations of MHD instabilities in clusters were carried out on *Deethought*,

the University of Maryland high performance computing cluster and on *jxb* at the École Normale Supérieure.

REFERENCES

- Balbus, S. A. 2000, *ApJ*, **534**, 420
 Balbus, S. A., & Reynolds, C. S. 2008, *ApJ*, **681**, L65
 Best, P. N., von der Linden, A., Kauffmann, G., Heckman, T. M., & Kaiser, C. R. 2007, *MNRAS*, **379**, 894
 Binney, J., & Cowie, L. L. 1981, *ApJ*, **247**, 464
 Bregman, J. N., & David, L. P. 1988, *ApJ*, **326**, 639
 Brügggen, M., Scannapieco, E., & Heinz, S. 2009, *MNRAS*, **395**, 2210
 Conselice, C. J., Gallagher, J. S., III, & Wyse, R. F. G. 2001, *AJ*, **122**, 2281
 Fabian, A. C., Sanders, J. S., Crawford, C. S., Conselice, C. J., Gallagher, J. S., & Wyse, R. F. G. 2003, *MNRAS*, **344**, L48
 Fabian, A. C., Voigt, L. M., & Morris, R. G. 2002, *MNRAS*, **335**, L71
 Hatch, N. A., Crawford, C. S., Johnstone, R. M., & Fabian, A. C. 2006, *MNRAS*, **367**, 433
 Kim, W.-T., & Narayan, R. 2003, *ApJ*, **596**, 889
 Nagai, D., Kravtsov, A. V., & Vikhlinin, A. 2007, *ApJ*, **668**, 1
 Nulsen, P. E. J., Stewart, G. C., Fabian, A. C., Mushotzky, R. F., Holt, S. S., Ku, W. H.-M., & Malin, D. F. 1982, *MNRAS*, **199**, 1089
 Parrish, I. J., & Quataert, E. 2008, *ApJ*, **677**, L9
 Parrish, I. J., Quataert, E., & Sharma, P. 2009, *ApJ*, **703**, 96
 Parrish, I. J., & Stone, J. M. 2005, *ApJ*, **633**, 334
 Parrish, I. J., & Stone, J. M. 2007, *ApJ*, **664**, 135
 Parrish, I. J., Stone, J. M., & Lemaster, N. 2008, *ApJ*, **688**, 905
 Peterson, J. R., & Fabian, A. C. 2006, *Phys. Rep.*, **427**, 1
 Quataert, E. 2008, *ApJ*, **673**, 758
 Reynolds, C. S., McKernan, B., Fabian, A. C., Stone, J. M., & Vernaleo, J. C. 2005, *MNRAS*, **357**, 242
 Ruszkowski, M., Enßlin, T. A., Brügggen, M., Heinz, S., & Pfrommer, C. 2007, *MNRAS*, **378**, 662
 Sharma, P., & Hammett, G. W. 2007, *J. Comput. Phys.*, **227**, 123
 Spitzer, L. 1962, *Physics of Fully Ionized Gases* (2nd ed.; New York: Interscience)
 Stone, J. M., Gardiner, T. A., Teuben, P., Hawley, J. F., & Simon, J. B. 2008, *ApJS*, **178**, 137
 Tozzi, P., & Norman, C. 2001, *ApJ*, **546**, 63
 Vernaleo, J. C., & Reynolds, C. S. 2006, *ApJ*, **645**, 83
 Voigt, L. M., Schmidt, R. W., Fabian, A. C., Allen, S. W., & Johnstone, R. M. 2002, *MNRAS*, **335**, L7
 Zakamska, N. L., & Narayan, R. 2003, *ApJ*, **582**, 162